

# We are IntechOpen, the world's leading publisher of Open Access books Built by scientists, for scientists

6,900

Open access books available

186,000

International authors and editors

200M

Downloads

Our authors are among the

154

Countries delivered to

TOP 1%

most cited scientists

12.2%

Contributors from top 500 universities



WEB OF SCIENCE™

Selection of our books indexed in the Book Citation Index  
in Web of Science™ Core Collection (BKCI)

Interested in publishing with us?  
Contact [book.department@intechopen.com](mailto:book.department@intechopen.com)

Numbers displayed above are based on latest data collected.  
For more information visit [www.intechopen.com](http://www.intechopen.com)



## Inverse Methods on Small Punch Tests

Inés Peñuelas, Covadonga Betegón, Cristina Rodríguez and Javier Belzunce  
*University of Oviedo  
Spain*

### 1. Introduction

The characterization of the mechanical behaviour of structural materials, with the exception of material hardness, is a destructive procedure which requires direct extraction of test specimens from the component to analyse. Because this component needs to be operative, these specimens have to be as small as possible, in order not to affect the behaviour of the component and in order to allow easy reparation of the 'damaged' component. However, tests with miniaturized specimens are not defined in standards. Thus, the results obtained with these tests have to be interpreted in order to obtain the actual properties of the components from which the specimens have been extracted (Lucas et al., 2002). The small punch test (SPT) is very useful in all applications that require the characterization of the mechanical behaviour of structural materials or operational components without compromising their service (Lucon, 2001), as in the case of nuclear or thermal plants. Another application is the study of small testing zones. Thus, this test has been recently applied to the mechanical characterization of metallic coatings (Peñuelas et al, 2009) or the heat affected zone of welds (Rodriguez et al, 2009), which are practically impossible to characterize by means of the conventional mechanical tests.

Advance constitutive models frequently include parameters that have to be identified through numerical simulation of tests and mathematical optimization of variables, because they cannot often be directly measured in laboratory. In this paper, an inverse methodology for the identification of the mechanical and damage properties of structural steels has been developed. Thus, from the load-displacement curves obtained during the non-standard SPT, the mechanical and damage properties will be obtained. Moreover, this methodology also allows simulating the SP test with numerical methods.

Structural steels may exhibit creep behaviour and behave according to the Hollomon's law ( $\sigma = K \epsilon_p^n$ ). Besides, ductile fracture of metallic materials involves micro-void nucleation and growth, and final coalescence of neighbouring voids to create new surfaces of a macro-crack. The ductile failure process for porous materials is often modelled by means of the Gurson model (Gurson, 1977), which is one of the most widely known micro-mechanical models for ductile fracture, and describes the progressive degradation of material stress capacity. In this model, which is a modification of the von Mises one, an elastic-plastic matrix material is considered and a new internal variable, the void volume fraction,  $f$ , is introduced. Although the original Gurson model was later modified by many authors, particularly by Tvergaard and Needleman (Tvergaard, 1981; Tvergaard, 1982; Tvergaard & Needleman, 1984), the resultant model is not intrinsically able to predict coalescence, and is only capable of

simulating micro-void nucleation and growth. This deficiency is solved by introducing an empirical void coalescence criterion: coalescence occurs when a critical void volume fraction,  $f_c$ , is reached (Tvergaard, 1982; Koplik & Needleman, 1998; Sun et al. 1992). Combining these models, it is possible to simulate the behaviour of materials from the elastic behaviour until their total fracture. The macromechanical and micromechanical parameters relate with different zones of the load-displacement curve obtained with the SPTs. These zones will be described below.

In the inverse procedure considered here, most data are pseudo-experimental data, that is, they are obtained from the numerical simulation of the test for a prescribed set of material parameters. Notwithstanding, many real experimental data are also considered in order to validate the numerical model and the inverse methodology developed.

## 2. Inverse methodology

The methodology used in this paper is based on inverse methods (Stravroulakis et al., 2003), design of experiments (Kuehl, 2000; Montgomery, 1997), numerical simulations of tests, least-squares polynomial regression for curve fitting and evolutionary genetic algorithms (Deb, 2001; Seshadri, 2006). Inverse problems lead to difficult optimization problems whose solutions are not always straightforward with current numerical optimization techniques. Therefore, one should consider semi-empirical methods and experimental testing techniques as well (Bolzon et al., 1997). Design of experiments (DOE) is the methodology of how to conduct and plan experiments in order to extract the maximum amount of information in the fewest number of runs. The statistical experiment designs most widely used in optimization experiments are termed response surface designs (Myers & Montgomery, 1995). In addition to trials at the extreme level settings of the variables, response surface designs contain trials in which one or more of the variables is set at the midpoint of the study range (other levels in the interior of the range may also be represented). Thus, these designs provide information on direct effects, pair wise interaction effects and curvilinear variable effects. Properly designed and executed experiments will generate more precise data while using substantially fewer experimental runs than alternative approaches. They will lead to results that can be interpreted using relatively simple statistical techniques. If there are curvilinear effects the factorial design can be expanded to allow estimation of the response surface. One way to do this is to add experimental points. The central composed design uses the factorial design as the base and adds what are known as star points. Special methods are available to calculate these star points, which provide desirable statistical properties to the study results.

In the inverse methodology, for the numerical and experimental tests, the different zones of the load-displacement curve have to be fitted. Data fitting is usually done by means of an error minimization technique, where the distance between parameterized predictions of the mechanical model (parameterized by the unknown parameters) and measurements of the corresponding experiment is minimized. This formulation is known as an output error minimization procedure for the inverse problem (Stravroulakis et al., 2003). In order to choose the best fitting model for all of them, for each fitting model, different statistical coefficients have been analysed:

1. The coefficient of multiple determination, also called proportion of variance explained  $R^2$ , that indicates how much better the function predicts the dependent variable than

- just using the mean value of the dependent variable (the closer to 1.0 (100%), the best the function predicts the observed data);
2. The adjusted coefficient of multiple determination  $R_a^2$  that is an  $R^2$  statistic adjusted for the number of parameters in the equation and the number of data observed (the closer to 1.0 the best the function predicts the observed data);
  3. The Durbin-Watson statistic, used to detect the presence of autocorrelation in the residuals from the regression analyses (a value less than 0.8 usually indicates that autocorrelation is likely (autocorrelation should be avoid));
  4. The t-ratio, that is a measure of the likelihood that the actual value of the parameter is not zero (the larger the absolute value of  $t$ , the less likely that the actual value of the parameter could be zero) and
  5. The prob( $t$ ) value that is the probability of obtaining the estimated value of the parameter if the actual parameter value is zero (the smaller the value of prob( $t$ ), the more significant the parameter and the less likely that the actual parameter value is zero).

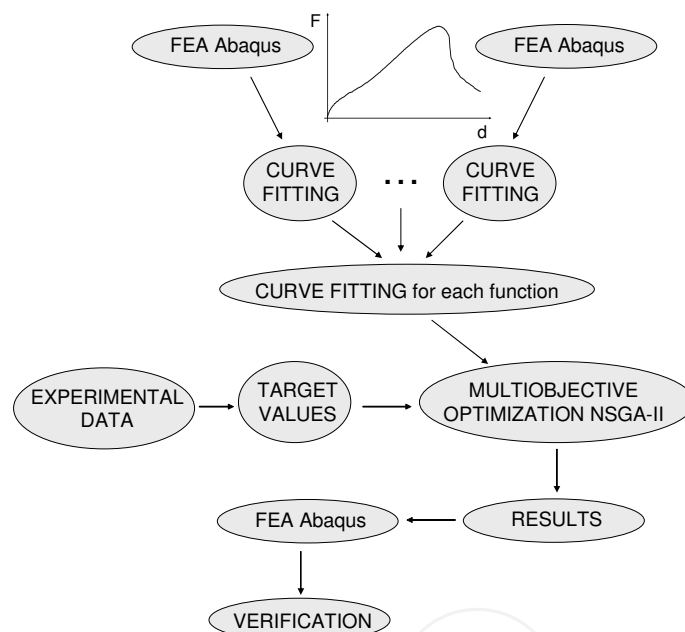


Fig. 1. Scheme for the inverse procedure

Inverse procedure finishes with the determination of the set of variable values that are associated to certain target values, obtained from the load-displacement curve of a laboratory SPT. That is, it has to be searched the set of variable values that simultaneously minimize a certain number of objective functions. This is a multiobjective optimization problem that can be solved using different procedures. In this paper, the Pareto front has been obtained by means of the evolutionary genetic algorithm NSGA-II (Seshadri, 2006). Pareto front produces non-dominated set of solutions with regard to all objectives and all solutions on the Pareto front are optimal. Besides, NSGA-II is non-domination based genetic algorithm which incorporates elitism (only the best individuals are selected) and that does not require choosing *a priori* sharing parameters. This algorithm is run in MATLAB. First of all the population is initialized based on the problem range and constraints if any. This population is sorted based on no domination (an individual is said to dominate another if

the objective functions of it, is no worse than the other and at least in one of its objective functions it is better than the other). Once the non-dominated sort is complete, a crowding distance, that is a measure of how close and individual is to its neighbours, is assigned. Parents are selected from the population by using binary tournament selection based on the rank and crowding distance. The selected population generates offspring from crossover and mutation operators. The population with the current population and current offspring is sorted again based on non-domination and only the best  $N$  individuals are selected, where  $N$  is the population size. Fig. 1 shows the scheme for the inverse procedure used for the material characterisation.

### 3. Small punch test (SPT)

By virtue of the small size of the specimens required for testing, the Small Punch Test can be considered a non-destructive test. Usually, the specimens used for the SPT are square plates of  $10 \times 10 \text{ mm}^2$  and just 0.5 mm thickness, although lower or higher thickness can also be used. In comparison with other non-destructive techniques such as ultrasonic or magnetic techniques and X-Rays, that are based on indirect measures for the determination of the above mentioned properties, the SPT allows obtaining directly the main mechanical properties of the materials.

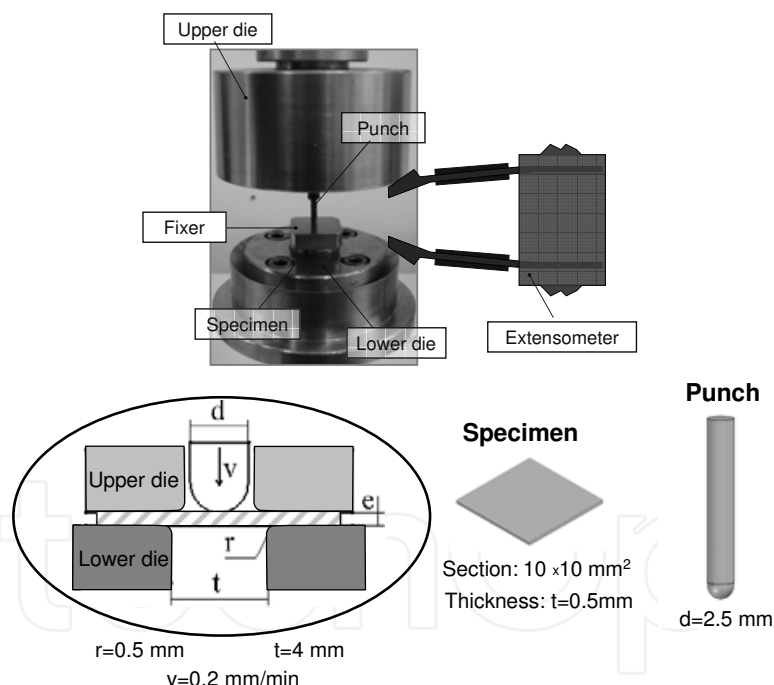


Fig. 2. Dispositive and geometry of the small punch test

In laboratory, the SPTs have been carried out with a low speed tensile test machine. Test consists of fixing the periphery of the specimen, embedding it between two dies (upper and lower dies) by means of four screws and a tightening torque of 2 N·m, and then deforming the specimen until its fracture by means of a small semi-spherical punch with a head of 2.5 mm of diameter. The test is speed controlled with a punching speed  $v = 0.2 \text{ mm/min}$ . In this way, the specimen is bounded to deform quasi-statically inside a 4 mm diameter hole (biaxial expansion) up to failure (Fig. 2). The data sampling rate during the experiment is 20

samples/s. Moreover, the test is finalized when load decreases the 50% of the maximum load.

By means of an extensometer, the displacement of the punch is obtained, and after correction of the flexibility of the testing device, the displacement of the central point of the specimen is calculated. Thus, from test is obtained the characteristic curve of material. This curve represents the force exerted from punch against the specimen (i.e. the load reaction) versus the displacement of the punch (Fig. 3). In the case of ductile materials, six different zones can be distinguished in these load-displacement curves obtained by means of the SPTs: zone I (elastic deformation), zone II (elastoplastic transition), zone III (generalized plastic deformation), zone IV (plastic instability and fracture initiation), zone V (fracture softening zone) and zone VI (final fracture).

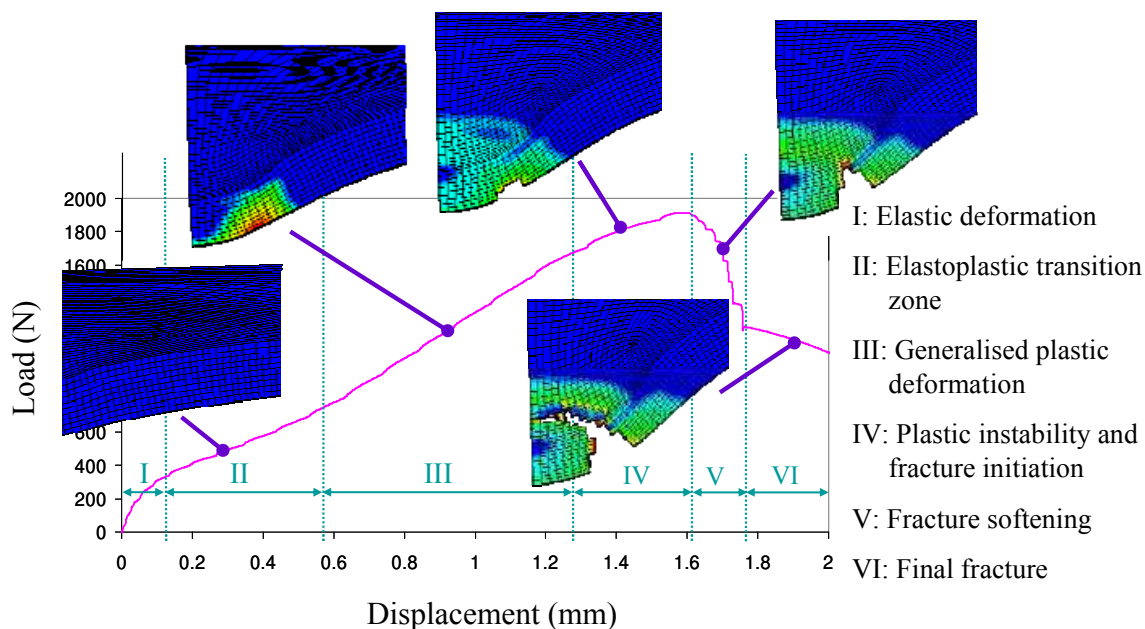


Fig. 3. Load-displacement curve for the SPT and Finite Element simulation at each zone

#### 4. Numerical simulation of the SPT

Different models have been developed in order to reproduce the SPTs by means of numerical methods. These models were compared with the aim of choosing the optimum model from the point of view of the relation between the precision and the computational cost. The numerical simulations have been carried out with the finite element commercial code ABAQUS (ABAQUS 6.7, 2008). In order to simulate the fracture behaviour of isotropic and anisotropic materials, two different meshes have been used (2D and 3D meshes, respectively). As it was pointed out before, the specimens for laboratory are squared specimens. However, because the hollow between the die and the specimen is a cylinder, the problem can be considered axisymmetric in the isotropic model, and the model can be solved by 2D axisymmetric meshes. Besides, for isotropic materials the 3D model has been compared with the axisymmetric one (2D) in order to justify the use of the axisymmetric model for the sake of simplicity. In the 2D-Axysim model, the specimens were discretised by means of an axisymmetric mesh of four-node reduced integration hybrid elements.

Notwithstanding, since many structural steels are obtained from lamination processes, they exhibit anisotropic behaviour. In these cases, three-dimensional meshes which reproduced a quarter of the specimen were used (Fig. 4). Although geometries of Fig. 4 appear to be different, the applied boundary conditions allow using both of them for isotropic materials. In this figure, upper die is not represented in order to improve the visualization of the model. In all cases, die and punch were modelled as rigid bodies. Besides, contact between surfaces, quasistatic analysis and large displacements were taken into account.

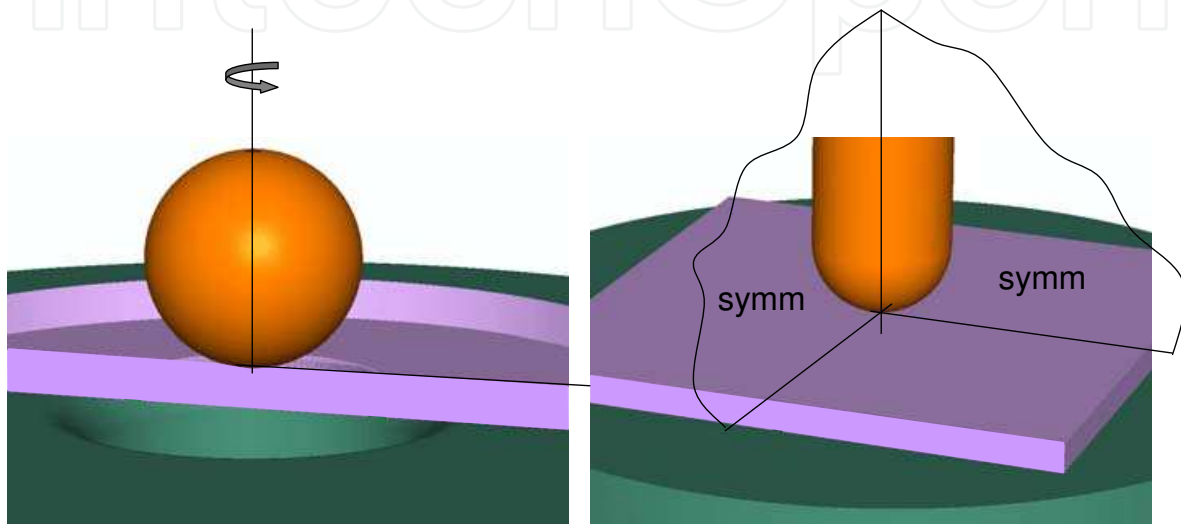


Fig. 4. Axysymmetric and Three-dimensional models used for the simulation of the SPT

From sensitivity analyses, it is observed that the elastic and elastoplastic transition zones (zones I and II of the load-displacement curve) are enough to characterize the macromechanical behaviour of steels that exhibit creep behaviour and follow the Hollomon's law ( $\sigma = K \epsilon_n^p$ ), whereas the remaining zones allow to characterize the micromechanical behaviour of the material and the coefficient of friction to be used in simulations.

In order to choose a value for the coefficient of friction, different simulations of known materials have been carried out. A good approximation has been obtained with  $\mu = 0.1$ , which is also an adequate value for steel-steel contact under partial lubrication. In the case of tests carried out with no lubrication, better results have been obtained with  $\mu = 0.25-0.35$ . These values have been obtained by comparing the experimental curve for an already known material (characterized by means of standard tests) with numerical ones obtained by means of the test simulation of this material with different values of coefficient of friction.

To describe the evolution of void growth and subsequent macroscopic material softening, the yield function of Gurson modified by and Tvergaard and Needleman (Tvergaard & Needleman, 1984) was used in this work. This modified yield function is defined by an expression in the form

$$\Phi(q, p, \bar{\sigma}, f) = \left(\frac{q}{\bar{\sigma}}\right)^2 + 2 \cdot q_1 \cdot f^* \cdot \cosh\left(-\frac{3 \cdot q_2 \cdot p}{2 \cdot \bar{\sigma}}\right) - (1 + q_3 \cdot f^{*2}) = 0 \quad (1)$$

where  $\bar{\sigma}$  is flow stress of the matrix material which relates with the equivalent plastic strain,  $f$  is the current void volume fraction,  $p = -\sigma_m$  with  $\sigma_m$  the macroscopic mean stress and  $q$  is the macroscopic von Mises effective stress given by

$$q = \sqrt{\frac{3}{2} \cdot (S_{ij} \cdot S_{ij})} \quad (2)$$

where  $S_{ij}$  denotes the deviatoric components of the Cauchy stress tensor. Constants  $q_1$ ,  $q_2$  and  $q_3$  are fitting parameters introduced by Tvegaard (Tvegaard, 1981; Tvegaard, 1982) to provide better agreement with results of detailed unit cell calculations. The modified void volume fraction,  $f^*$ , was introduced by Tvegaard and Needleman (Tvegaard & Needleman, 1984) to predict the rapid loss in strength that accompanies void coalescence, and is given by

$$f^* = \begin{cases} f & \text{si } f \leq f_c \\ f_c + \frac{f_u^* - f_c}{f_f - f_c} \cdot (f - f_c) & \text{si } f > f_c \end{cases} \quad (3)$$

where  $f_c$  is the critical void volume fraction,  $f_f$  is the void volume fraction at final failure which is usually  $f_f = 0.15$  and  $f_u^* = 1/q_1$  is the ultimate void volume fraction.

The internal variables of the constitutive model are  $\bar{\sigma}$  and  $f$ . Thus the evolution law for the void volume fraction is given in the model by an expression in the form

$$\dot{f} = \dot{f}_{\text{growth}} + \dot{f}_{\text{nucleation}} \quad (4)$$

The void nucleation law implemented in the current model takes into account nucleation of both small and large inclusions. The nucleation of larger inclusions is stress controlled, and it is assumed that larger inclusions are nucleated at the beginning of the plastic deformation, being considered as initial void volume fraction. The nucleation of smaller inclusions is strain controlled and, accordingly to Chu and Needleman (Chu & Needleman, 1980) the nucleation rate is assumed to follow a Gaussian distribution, that is

$$\dot{f}_{\text{nucleation small particles}} = A \cdot \dot{\bar{\epsilon}}^p \quad (5)$$

where  $\dot{\bar{\epsilon}}^p$  is the equivalent plastic strain rate, and

$$A = \frac{f_n}{S_n \cdot \sqrt{2 \cdot \Pi}} \cdot \exp\left(-\frac{1}{2} \cdot \left(\frac{\bar{\epsilon}^p - \epsilon_n}{S_n}\right)^2\right) \quad (6)$$

where  $S_n$  is the standard deviation,  $\epsilon_n$  is the mean strain and  $f_n$  is the void volume fraction of nucleating particles.

The growth rate of the existing voids can be expressed as a function of the plastic strain rate in the form

$$\dot{f}_{\text{growth}} = (1 - f) \cdot \dot{\epsilon}_{kk}^p, \quad (7)$$

where  $\dot{\epsilon}_{ij}^p$  is the plastic strain rate tensor.

## 5. Model calibration and sensitivity analysis

Prior to the inverse procedure is the direct adjustment of the numerical simulation and the experimental test for a small number of materials previously characterized by standard tests. That is the model calibration and it requires the determination of the unknown parameters of the model, especially of the ones relevant to defects and damage, by comparing the results of the model with experimental measurements. Afterwards, the load-displacement curves obtained from laboratory SPT and from FE simulation of the test for a material previously characterized from standard specimens, are compared. Fig 5 shows the qualitative comparison of the experimental and numerical deformation shape and fracture zones of the axisymmetric model at the final fracture of the specimen.

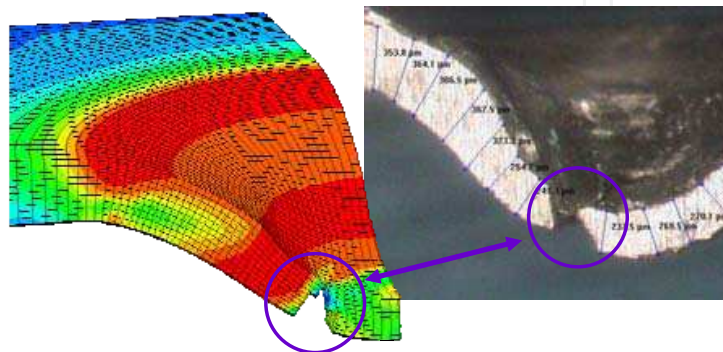


Fig. 5. Comparison of the experimental and numerical deformation shape and fracture zones of a SPT specimen

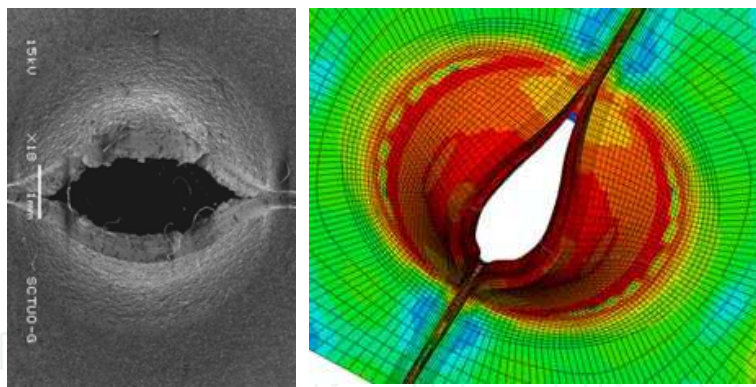


Fig. 6. Comparison of the experimental and numerical deformation shape and fracture zones of a notched SPT specimen

Moreover, Fig. 6 shows the comparison of deformation and overall appearance of the fracture zone obtained by a laboratory test and the numerical simulation, for SPT specimen with a longitudinal notch. In the case of notched specimens, 3D models has been used. It has been found very good correlation between tests and simulations, not only for the un-notched specimens but also for the notched specimens.

After setting the model, and before beginning the process of characterization, it is necessary to study which variables influence each of the zones of the load-displacement curve. For this purpose, several numerical simulations have been carried out. Fig. 7 shows the material parameters (variables to determine) that affect each zone of the load-displacement curve, obtained by means of SP tests.

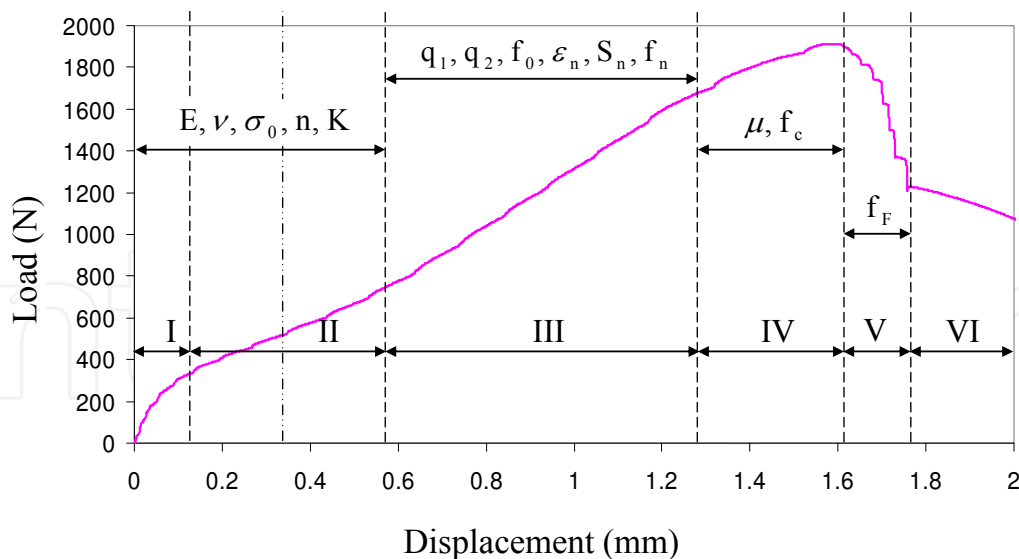


Fig. 7. Load-displacement curve of the SPT and parameters that affect each zone

From sensitivity analyses ( $\pm 10\%$ ), it has been shown that load-displacement curves are very sensitive to variations in  $n$  and  $K$  (along the entire curve) and less sensitive to variations in  $\sigma_0$  (which mainly affects zone II). Moreover, since the SPT specimens reach the elastoplastic regime in the early stages of testing, the effect of Young's modulus is very small, so that  $E$  can be considered a constant reference value for all materials tested (analysed). Although the thickness of the specimen is a variable that has considerable influence on the load-displacement curve, in order to characterize the material is desirable using constant thickness. Therefore in Figure 7 is not shown the variable thickness-of-the-specimen. On the other hand, since the database has been obtained from pseudo-experimental data (numerical simulations), the technical problem of cutting all the specimens to the same small thickness (0.5 mm) is eliminated. Thus, for all simulations has been considered a fixed thickness.

## 6. Characterization methodology and results

As it was pointed out before, prior to the inverse procedure is the model calibration and the sensitivity analysis for the main variables. Afterwards, the inverse characterization scheme is applied. The complete material characterization requires the determination of a high number of parameters: coefficient of friction ( $\mu$ ), Young's modulus or elastic modulus ( $E$ ), Poisson's ratio ( $\nu$ ), yield stress ( $\sigma_0$ ), strain hardening exponent ( $n$ ), Hollomon's factor ( $K$ ), fitting parameters introduced by Tvergaard and Needleman for the GTN yield potential ( $q_1$ ,  $q_2$  and  $q_3$ ), initial void volume fraction ( $f_0$ ), mean strain in the Gaussian distribution of the nucleation rate ( $\varepsilon_n$ ), standard deviation in the Gaussian distribution of the nucleation rate ( $S_n$ ), void volume fraction of nucleating particles in the Gaussian distribution of the nucleation rate ( $f_n$ ), critical void volume fraction ( $f_c$ ) and void volume fraction at final failure ( $f_F$ ). However, some of them can be obtained from literature or from previous works. This is the case for the  $\mu$ ,  $E$ ,  $\nu$ ,  $q_1$ ,  $q_2$ ,  $q_3$ ,  $f_0$ ,  $S_n$  parameters. For metallic materials (structural steels) usual values of these constants are:  $E=2e5$  MPa,  $\nu = 0.3$ ,  $q_1 = 1.5$ ,  $q_2 = 1.0$ ,  $q_3 = q_1^2 = 2.25$  and  $S_n = 0.01$  (small values of  $S_n$  relate to quite homogeneous materials). From metallographic observation of experimental specimens, the initial porosity has been considered  $f_0 = 0$ . And finally, from previous adjustments  $\mu=0.1$ . Once the previous parameters are set, the number

of parameters to determine has been strongly reduced from 15 to 7:  $\sigma_0$ ,  $n$ ,  $K$ ,  $\varepsilon_{iv}$ ,  $f_{iv}$ ,  $f_c$  and  $f_F$ . The first three parameters are macromechanic ones, the rest are micromechanic parameters for the damage model.

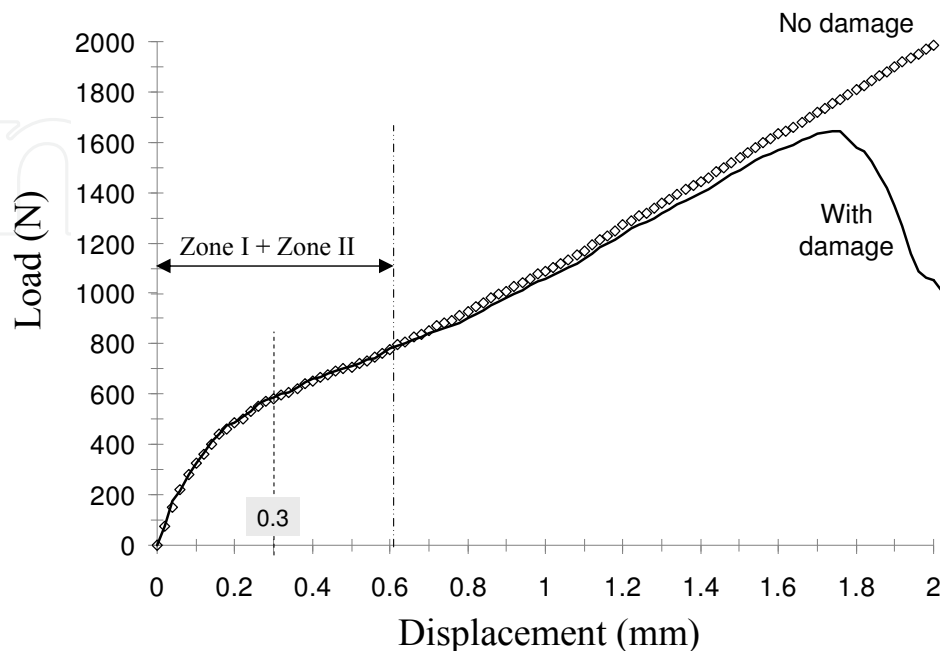


Fig. 8. Comparison of the Load-displacement curves with and without taking into account the damage of material

Since the damage parameters have no influence in the elastic and elastoplastic transition zones of the load-displacement curve (zones I and II), is possible to uncouple the macromechanical and the micromechanical characterizations. For this reason two different phases have been used for the macro- and micromechanical characterizations. First of all, the material has been macromechanically characterized by means of the analysis of zones I and II of the load-displacement curve. Then, the micromechanical parameters for the previously macro-characterized material have been determined using the remaining zones of the curve. Figure 8 shows the comparison between two numerical simulations for the same material with and without consideration of the damage model.

### 6.1 Macromechanical characterization

All inverse procedure requires a sufficiently large number of experimental data or pseudo-experimental data (numerical simulations). These data consist on sets of input variables for the macromechanical characterization ( $E$ ,  $\nu$ ,  $\sigma_0$ ,  $n$ ,  $K$ ) and output data obtained from the load-displacement curves. As it was pointed out before, the elastic modulus and the Poisson's ratio can be considered beforehand known. Thus for a certain fixed values of the elastic modulus  $E = 2e5$  MPa and the Poisson's ratio  $\nu = 0.3$ , different combinations of ( $\sigma_0$ ,  $n$ ,  $K$ ) have to be defined. In this paper, two different types of input variables have been taken into account. On the one hand, the design of experiments has been applied in order to define a small set of tests to simulate (15 tests). Thus, in order to identify the values of these sets of variables to simulate, it has been used design of experiments central composed centred on body, based on quadratic response surfaces. On the other hand, a wide battery of numerical

simulations (180 simulations) has been used not only to characterize the material macromechanically but also to quantify the effect of the simplifications inherent to the design of experiments. Besides, this battery is suitable for a wide range of structural steels. In both cases, the input variables vary within the following ranges

$$\sigma_0 = 200 - 700 \text{ MPa}, n = 0.1 - 0.3 \quad (8)$$

$$K = \begin{cases} 1.5 \cdot \sigma_0 - 3.5 \cdot \sigma_0 & \text{if } 0.1 \leq n < 0.15 \\ 2.0 \cdot \sigma_0 - 4.0 \cdot \sigma_0 & \text{if } 0.15 \leq n < 0.2 \\ 2.5 \cdot \sigma_0 - 4.5 \cdot \sigma_0 & \text{if } 0.2 \leq n < 0.25 \\ 3.0 \cdot \sigma_0 - 5.0 \cdot \sigma_0 & \text{if } 0.25 \leq n < 0.3 \end{cases} \quad (9)$$

In the case of using the battery of numerical simulations, the maximum variation of  $(\sigma_0, n)$  is  $\Delta(\sigma_0, n)_{\max} = (50 \text{ MPa}, 0.01)$ .

In the design of experiments, it was considered a new variable  $K^*$  in order to correctly define the sets of values for simulation. This variable  $K^*$  varies from 1.5 to 3.5 and is given by

$$K^* = \left( \frac{K}{\sigma_0} - 0.5 \cdot i \right) \quad (10)$$

where  $i$  is defined by

$$i = \begin{cases} 0 & \text{if } 0.1 \leq n < 0.15 \\ 1 & \text{if } 0.15 \leq n < 0.2 \\ 2 & \text{if } 0.2 \leq n < 0.25 \\ 3 & \text{if } 0.25 \leq n < 0.3 \end{cases} \quad (11)$$

The output data were obtained from the curve fitting of zones I and II of the load-displacement curve in a two stage procedure which consists of:

1. First, fixing the range of displacement for the analyze. For all the structural steels simulated (180 steels with mechanical properties varying within the ranges defined before), a displacement value that has been proved to provided good results is 0.3 mm.
2. Then, adjusting the zone I and part of the zone II with an unique mathematical law. A commercial software, DataFit (DataFit 8.2, 2009) has been used for this purpose. The best fitting model is chosen by analyzing the different statistical coefficients of the different models. From the analysis of the different statistical coefficients of the different models, the best fitting model has been chosen. This consists in a exponential law in the form  $y = \exp(a + b/x + c \cdot \ln(x))$ , where  $y$  corresponds to load and  $x$  correspond to displacement. Fig. 9 shows this curve fitting for a generic material. In this way, the three output data obtained from each set of input data are the factors  $a$ ,  $b$ ,  $c$ , which depend on the three variables to determine, that is  $a = a(\sigma_0, n, K)$ ,  $b = b(\sigma_0, n, K)$  and  $c = c(\sigma_0, n, K)$ .

Each of these functions is postulated as a polynomial model (Cuesta et al., 2007), being necessary determining its order. The higher this order, the bigger the number of coefficients to determine. Thus, in a second-order model the number of coefficients to determine is 10; in a third-order model is 20 and in a fourth-order model is 31. By the comparison of the numerical results obtained by the method of least-squares, and polynomial regressions of

orders two, three and four, it has been chosen to use the following models for the functions a,b,c: second-order models in case of using DOE for simulations and third-order models in case of using the battery of simulations, since they allow to reach good-enough adjustments using a relatively small number of coefficients. Table 1 gives detail of the  $R_a^2$  values for each function a, b, c obtained with models of different orders. From this table can be observed that the adjusted coefficient of multiple determination is much higher for the battery of numerical simulations (180 simulations) than for the design of experiments (15 simulations). Besides, all the regressions used are very significant and the proportion of variance of a, b, c, explained are 99.7%, 95.6% and 98.4%, respectively.

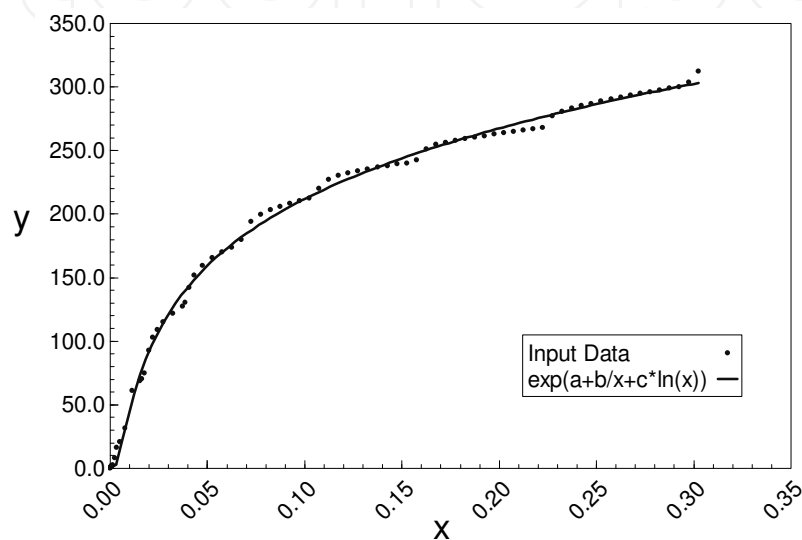


Fig. 9. Exponential adjustment of the Load-displacement curve in zone (I+II) until  $d=0.3$  mm. Moreover, it has been carried out sensitivity analyses within a  $\pm 10\%$  variation of the factors a, b, c of the exponential law, in order to analyse their effect on the load-displacement curve. These analyses show that the influence of the function a on the exponential law is enormous, the influence of c is notable and the influence of b is not important.

	Design of experiments	Battery of numerical simulations		
	2 <sup>nd</sup> order	2 <sup>nd</sup> order	3 <sup>er</sup> order	4 <sup>th</sup> order
a	0.981	0.986	0.997	0.999
b	0.889	0.934	0.951	0.960
c	0.907	0.961	0.982	0.987

Table 1.  $R_a^2$  coefficients for functions a, b and c

In case of using design of experiments, the second order polynomial models for functions a, b and c can be write by expressions in the form

$$g(\sigma_0, n, K) = g_0 + g_1 \cdot \sigma_0 + g_2 \cdot n + g_3 \cdot K + g_{11} \cdot \sigma_0^2 + g_{22} \cdot n^2 + g_{33} \cdot K^2 + g_{12} \cdot \sigma_0 \cdot n + g_{13} \cdot \sigma_0 \cdot K + g_{23} \cdot n \cdot K \quad (12)$$

where  $g(\sigma_0, n, K)$  correspond to  $a=a(\sigma_0, n, K)$ ,  $b=b(\sigma_0, n, K)$  and  $c=c(\sigma_0, n, K)$ .

Similarly, in the case of using the battery of numerical simulations, the third-order polynomial models for each function can be expressed in the form

$$\begin{aligned}
g(\sigma_0, n, K) = & g_0 + g_1 \cdot \sigma_0 + g_2 \cdot n + g_3 \cdot K + g_{11} \cdot \sigma_0^2 + g_{22} \cdot n^2 + g_{33} \cdot K^2 + g_{12} \cdot \sigma_0 \cdot n + g_{13} \cdot \sigma_0 \cdot K + \\
& + g_{23} \cdot n \cdot K + g_{123} \cdot \sigma_0 \cdot n \cdot K + g_{112} \cdot \sigma_0^2 \cdot n + g_{113} \cdot \sigma_0^2 \cdot K + g_{122} \cdot \sigma_0 \cdot n^2 + g_{223} \cdot n^2 \cdot K + \\
& + g_{133} \cdot \sigma_0 \cdot K^2 + g_{233} \cdot n \cdot K^2 + g_{111} \cdot \sigma_0^3 + g_{222} \cdot n^3 + g_{333} \cdot K^3
\end{aligned} \quad (13)$$

Coefficients  $g_{ijk}$  have been obtained using the commercial software DataFit with regularized input values  $(\sigma_0, n, K)$  varying within the range  $[0, 1]$ . Values obtained for a 99% confidence interval are shown in Table 2.

	a	b	c
$g_0$	5.71048018	-0.00829258	0.25978748
$g_1$	0.00191446	-0.01508759	-0.36809281
$g_2$	-0.60585504	-0.00051838	-0.0886477
$g_3$	6.75259819	0.02658378	1.38774367
$g_{11}$	1.45337999	-0.00480519	0.33279479
$g_{22}$	-0.17753184	-0.0056283	-0.11501128
$g_{33}$	-2.88944339	-0.09971593	-1.81039397
$g_{12}$	0.00491019	-0.02896433	-0.48577964
$g_{13}$	-5.52592006	0.06567327	0.1338645
$g_{23}$	-1.12143967	0.04558742	0.55393563
$g_{123}$	-5.13987844	-0.06643944	-2.1955321
$g_{112}$	1.11391405	0.02857506	0.75839976
$g_{113}$	-1.44430745	-0.10182755	-1.94692201
$g_{122}$	1.40276526	0.00766641	0.38699445
$g_{223}$	-2.58686787	-0.01189609	-0.60625958
$g_{133}$	9.53781127	0.14445698	4.01278162
$g_{233}$	6.71653262	0.04137906	1.80579095
$g_{111}$	-0.47228307	0.01499177	0.10613477
$g_{222}$	0.42619501	0.00050424	0.0751837
$g_{333}$	-5.67785877	-0.04182362	-1.71486231

Table 2.  $g_{ijk}$  coefficients for the third- order models for functions a, b and c

Finally, the inverse procedure finishes with the multiobjective optimization. That is, with the determination of the set of values  $(\sigma_0, n, K)$  that are associated to target values, which were obtained from the load-displacement curve of a specific laboratory small punch test. In our case,  $a_{\text{target}}=-6.097034$ ,  $b_{\text{target}}=0.009365$  and  $c_{\text{target}}=0.283507$ . Therefore, it have to be searched the set of variable values that simultaneously minimize three target (objective) functions:  $(a - a_{\text{target}})$ ,  $(b - b_{\text{target}})$  and  $(c - c_{\text{target}})$ . This multiobjective optimization problem has been solved using the evolutionary genetic algorithm NSGA-II, which has been run in MATLAB (MATLAB, 2006). The input arguments for the function `nsga_2`, are the population size and

number of generations. In this paper, the population size has been set to 200 and the number of generations has been set to 100. Since the algorithm incorporates elitism, only the best  $N$  individuals are selected, where  $N$  is the population size. The process repeats to generate the subsequent generations (100 generations). With this procedure the Pareto front is obtained, and it is represented in the space of functions  $[(a - a_{\text{target}}), (b - b_{\text{target}}), (c - c_{\text{target}})]$ . Fig. 10 shows the Pareto front in the space of functions for the target values.

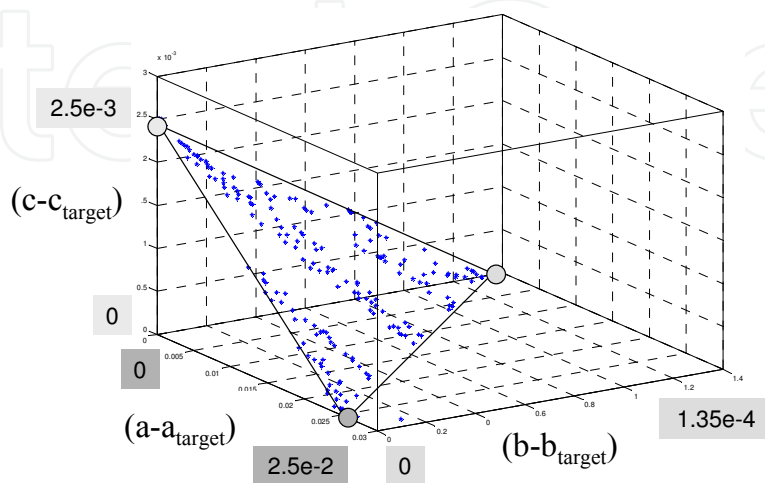


Fig. 10. Pareto front (Zone I+II) in the space of functions for the target values

As it was pointed out before, Pareto front produces non-dominated set of solutions with regard to all objectives and all solutions on the Pareto front are optimal. Furthermore, sensitivity analyses in functions  $a$ ,  $b$  and  $c$  has shown that the variable that affects more the load-displacement curve (that is, the result) is variable  $a$ . As a result, from all the possible solutions that form the Pareto front, should be chosen those that show lower values of function objective  $(a - a_{\text{target}})$ . Fig. 11 shows the Pareto front in the space of solutions for the target values. Within this values it has been chosen one in the zone with higher population density of the solution space  $(\sigma_0, n, K)$ , and it has been called the calculated set of variables  $(\sigma_0, n, K)_{\text{calculated}}$ . In order to verify its 'goodness', it has been compared with the values of the variables  $(\sigma_0, n, K)$  obtained by means of standard laboratory tests (traction test), which have been called the known values  $(\sigma_0, n, K)_{\text{known}}$ .

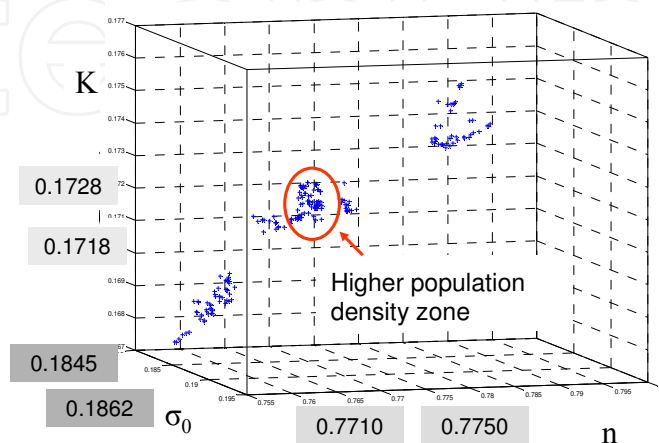


Fig. 11. Pareto front in the space of solutions

Moreover, the numerical simulation of the resulting values  $(\sigma_0, n, K)_{\text{calculated}}$  has been carried out in order to obtain the  $a, b, c$  parameters from the numerical load-displacement curve. These values have also been compared with the objective experimental values. Besides, the numerical and experimental load-displacement curves and the stress-strain curves have been compared too. Very good agreement has been observed in all cases. Table 3 gives detail of the comparison between the calculated values  $(\sigma_0, n, K)_{\text{calculated}}$  and those obtained with standard laboratory traction test  $(\sigma_0, n, K)_{\text{known}}$ . The relative error between the known and calculated values are also shown in Table 3.

Known values		Calculated	
		Value	Error (%)
$\sigma_0$	291.6	292.3	0.24
$n$	0.256	0.2548	0.47
$K$	854.5	849.76	0.55

Table 3. Results obtained and relative error

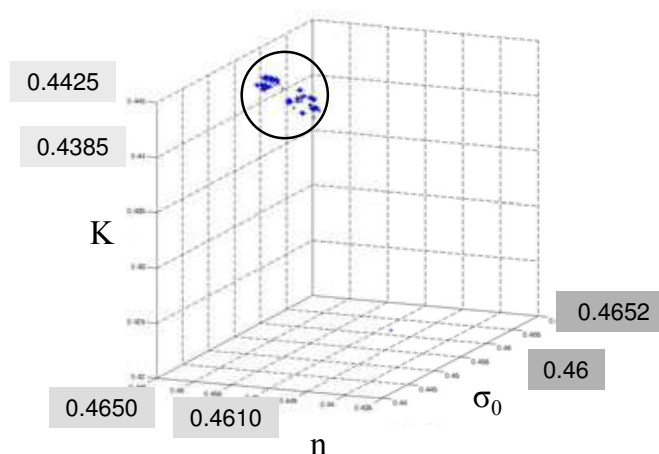


Fig. 12. Pareto front in the space of solutions for another material

Moreover, in Fig. 11 there are different zones with high population density (solutions). Thus, at a slight thought it could be thought that there is no uniqueness in solution, because there are different zones in the figure with high population density. This fact is however observed in some solutions, but generally it is not a problem, because the ranges of variation of variables in the different solutions and their influence on the stress-strain curve is small enough to consider that any result is a good one. However, in many other cases there is only a single zone with high population density and all values trend to a unique solution (Fig. 12)

## 6.2 Micromechanical characterization

Once the material has been macromechanically characterized, only four of the seven parameters to determine  $(\sigma_0, n, K, \varepsilon_n, f_n, f_c$  and  $f_f)$  are still unknown ( $\varepsilon_n, f_n, f_c$  and  $f_f)$  and they have to be obtained by means of another inverse procedure. The input variables for the micromechanical characterization are  $\varepsilon_n, f_n, f_c$  and  $f_f$ . From Fig. 7 it has been shown that the

only parameters to identify in zone III are  $\varepsilon_n$  and  $f_n$ . In this zone, central composed experiment design centred on faces, based on quadratic response surfaces, has been used to identify the values of these sets of variables to simulate and to choose the minimum number of sets required. In Zone III, only has been applied design of experiments, since defining multiple batteries of simulations for each particular material that it is not known beforehand, is not operative. It has been selected 20 sets of variables (20 experiments) distributed in order to obtain variable inflation factors greater than one and lower than four. In addition, the input variables vary within the following ranges

$$\varepsilon_n = 0.15 - 0.3, f_n = 0.01 - 0.07 \quad (14)$$

which are typical ranges for steels (Abendroth and Kuna, 2003). In addition, the maximum variation of  $(\varepsilon_n, f_n)$  is  $\Delta(\varepsilon_n, f_n)_{\max} = (0.05, 0.015)$ .

Zone III has been adjusted with a linear law in the form  $y=l+m \cdot x$ . Again, the commercial software DataFit has been used for this purpose. Now, the two output data obtained from each input set are the factors  $l$  and  $m$ , which depend on the two variables to determine, that is  $l=l(\varepsilon_n, f_n)$  and  $m=m(\varepsilon_n, f_n)$ . Both factors are postulated as second-order polynomial models that can be written in the form

$$g(\varepsilon_n, f_n) = g_0 + g_1 \cdot \varepsilon_n + g_2 \cdot f_n + g_{11} \cdot \varepsilon_n^2 + g_{22} \cdot f_n^2 + g_{12} \cdot \varepsilon_n \cdot f_n \quad (15)$$

where  $g(\varepsilon_n, f_n)$  correspond to  $l=l(\varepsilon_n, f_n)$  and  $m=m(\varepsilon_n, f_n)$ .

Coefficients  $g_{ij}$  have been obtained using DataFit with regularized input values  $(\varepsilon_n, f_n)$  varying within the range  $[-1, 1]$ . Table 4 gives detail of the values obtained for a 99% confidence interval. Both regressions are very significant and the proportion of variance of  $l$  and  $m$ , explained are 99.3%, 99.7%, respectively. From zone III of the load-displacement curve of the laboratory small punch test, the target values are  $l_{\text{target}}=0.0119$  and  $m_{\text{target}}=0.7909$ .

	l	m
$g_0$	0.022333	0.774075
$g_1$	-0.001755	0.011094
$g_2$	0.029950	-0.051640
$g_{11}$	-0.001519	0.001642
$g_{22}$	0.000071	0.000086
$g_{12}$	-0.00123	0.007788

Table 4.  $g_{ij}$ . coefficients for the second- order models for functions  $l$  and  $m$

Again, Pareto front has been obtained by means of the evolutionary genetic algorithm NSGA-II run in MATLAB. The Pareto front in the space of functions  $[(m - m_{\text{target}}), (l - l_{\text{target}})]$  for the target values is shown in Fig. 13. Moreover, Fig. 14 shows the Pareto front in the space of solutions  $(\varepsilon_n, f_n)$ . In order to verify its 'goodness', the numerical simulation of the resulting values  $(\varepsilon_n, f_n)_{\text{calculated}}$  has been carried out in order to obtain the  $(l, m)$  parameters from the numerical load-displacement curve

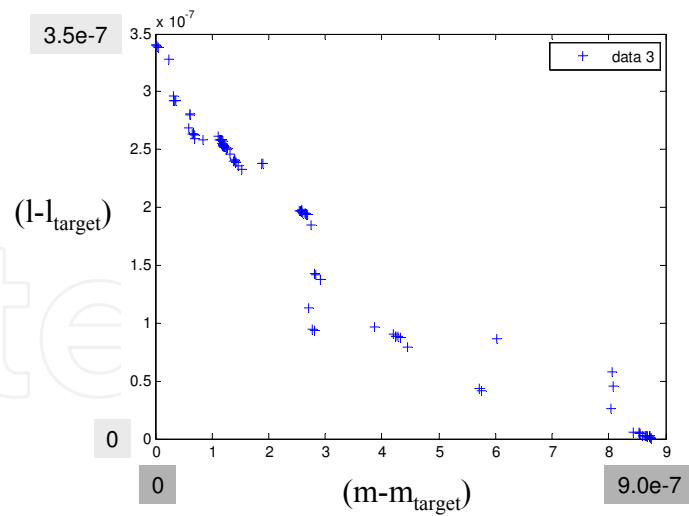


Fig. 13. Pareto front (Zone III) in the space of functions for the target values

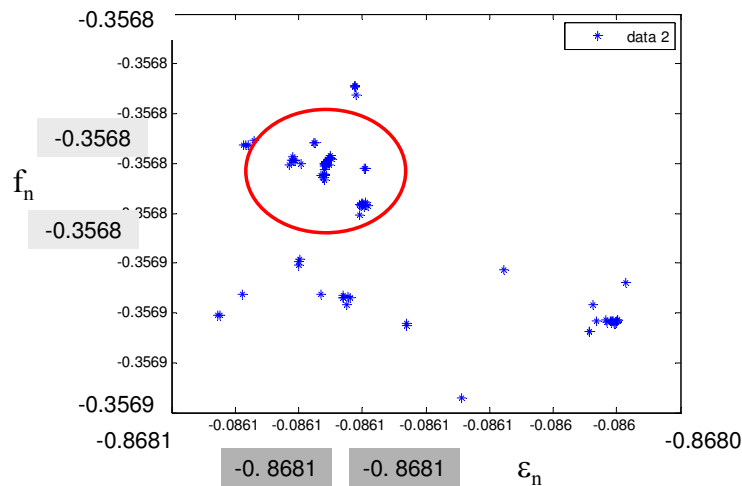


Fig. 14. Pareto front (Zone III) in the space of solutions

Calculated			
$\epsilon_n$	0.2107		
$f_n$	0.0293		
↓	Target	Pareto	Error (%)
l	0.0119	0.0119	1.78e-3
m	0.7909	0.7909	1.45e-4

Table 5. Results obtained for zone III and relative error

Table 5 gives detail of these values. This table also shows the relative error of the functions l and m with respect to the objective values  $(l,m)_{target}$ . Again, very good agreement has been observed in all cases.

Once the parameters  $\epsilon_n$  and  $f_n$  have been determined a very good agreement between the experimental and numerical curves at zones I, II and III has been achieved. However, it is

from zone IV where the curves separate from each other due to the accelerating effect on the evolution law of the void volume fraction induced from void coalescence, which seriously affect the load resistance capacity of the material. The critical void volume fraction  $f_c$  is the only parameter that defines the beginning of coalescence in the material. This value can be obtained from the evolution law of the void volume fraction of the specimen at the region where failure takes place. The value of  $f_c$  is the value of porosity (void volume fraction) at the instant in which the experimental and numerical curves begin to separate from each other, and corresponds to the initiation of Zone IV. For the target material (studied material), this separation takes place for a displacement of the punch of 1.32 mm. Thus, the corresponding critical void volume fraction obtained is  $f_c=0.07$  (Fig. 15).

After  $f_c$  has been determined, the void volume fraction keeps on growing up to the maximum load point. This maximum marks the beginning of zone V where the load carrying capacity decreases drastically. The slope of this zone depends on  $f_F$ . The value of  $f_F$  can be obtained carrying out several simulations with different values of  $f_F$  until the best agreement in zone V is obtained. For the material studied in this paper (tested by means of the SPT), very good agreement between the experimental and numerical curves is achieved with  $f_F=0.1$ .

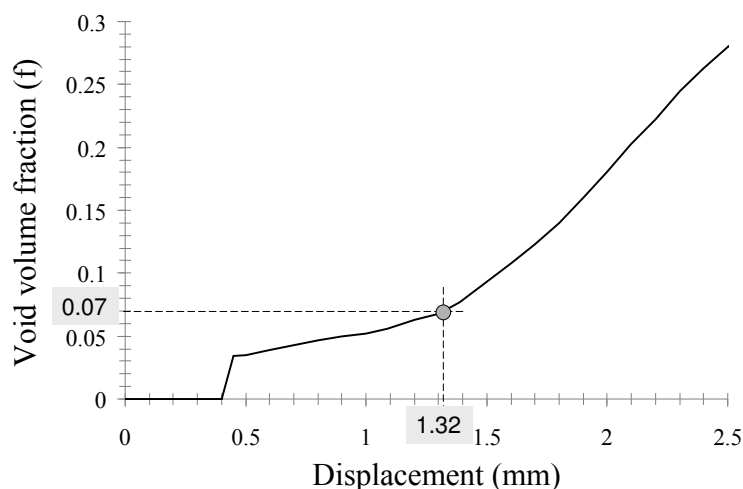


Fig. 15. Void volume fraction–displacement curve and onset of void coalescence

$\sigma_0$ (MPa)	$n$	$K$	$\epsilon_n$	$f_n$	$f_c$	$f_F$	$q_1$	$q_2$
292.3	0.2548	849.76	0.2107	0.0293	0.07	0.1	1.5	1.0
$q_3$	$f_0$	$S_n$	$\mu$	$E$ (MPa)	$\nu$			
2.25	0	0.01	0.3	200 000	0.3			

Table 6. Complete characterization for the studied material

Once the macromechanic characterization and the micromechanic characterization have been completed, the material is completely characterized. The resulting values for the different parameters obtained by means of the methodology presented in this paper for the complete characterization of the SP tested material are detailed (Table 6).

## 7. Conclusion

In this paper has been developed an inverse methodology for the determination of the mechanical and damage properties of structural steels that behave according to the Hollomon's law and to the damage model developed by Gurson, Tvergaard and Needleman. Most of these parameters have been derived from the load-displacement curve, which has been obtained by means of small punch tests.

This methodology allows:

1. To characterize not only macromechanically but micromechanically, a wide variety of structural steels, combining experimental data and pseudo-experimental data (numerical simulations).
2. Knowing the deformation of specimen while the test is running
3. To identify the zone of the load-displacement curve that is affected by each variable, and to perform sensitivity analyses.

Moreover, the Pareto front and the evolutionary genetic algorithms allow to obtain, in a relative easy way, numerical results that fit with good agreement the experimental results. In addition, the best way to tackle the parameter identification problem, seems to be the use of a battery of numerical simulations combined with design of experiments. The former has to be used for the macromechanical characterization, whereas the later should be used for the micromechanical characterization.

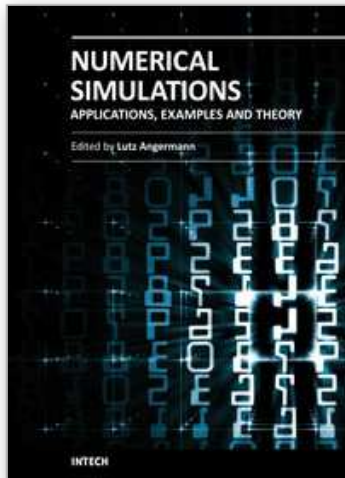
Finally, the inverse methodology shown in this paper, has to be developed for each type of material, as well as for each thickness of the specimen and each test temperature.

## 8. References

- Abendroth, M. and Kuna, M. (2003) Determination of deformation and failure properties of ductile materials by means of the small punch test and neural networks. *Comput. Mater. Sci.* 28, 633–644, ISSN: 0927-0256.
- Bolzoni, G. et al. (1997) *Parameter identification of the cohesive crack model Material Identification using Mixed Numerical Experimental Methods*, H. Sol and C. W. J. Oomens Ed., pp. 213–222, Kluwer Academic, Dordrecht, Netherlands.
- Chu, C. C. and Needleman, A. (1980) Void nucleation effects in biaxially stretched sheets. *J. Eng. Mat. Tech.* 1028, 249–256, ISSN: 0094-4289.
- Cuesta, I. I. et al. (2007) Determinación de los parámetros del modelo de daño de Gurson-Tvergaard para la simulación del ensayo de Small Punch. *Anales de Mecánica de la Fractura* 24, 429–434, ISSN: 0213-3725.
- DataFit 8.2. Oakdale engineering. Oakdale, California, USA.
- Deb, K. (2001). In: *Multiobjective Optimization using Evolutionary Algorithms*. JohnWiley & Sons, Chichester, UK.
- Gurson, A. L. (1977) Continuum theory of ductile rupture by void nucleation and growth: part I – yield criteria and flow rules for porous ductile media. *J. Eng. Mat. Tech.* 99, 2–15, ISSN: 0094-4289.
- Hibbit, Karlsson and Sorensen (2009) *ABAQUS 6.7*. Inc., Pawtucket, Rhode Island, USA.
- Koplik J & Needleman A. (1998) Void growth and coalescence in porous plastic solids. *Int J Solids Struct*;24, 835–53, ISSN: 0020-7683.
- Kuehl, R. O. (2000), In: *Design of Experiments*, 2nd edn. Thomson Learning, ISBN: 0-534-36834-4, Duxbury, Massachusetts, USA.

- Lucas, G. E., Odette, G. R., Sokolov, M., Spätig, P., Yamamoto, T. & Jung, P. (2002). Recent progress in small specimen test technology. *J. Nucl. Mater.* 307-311, 1600-1608, ISSN: 0022-3115.
- Lucon, E. (2001) Material damage evaluation and residual life assessment of primary power plant components using specimens of non-standard dimensions. *Mater. Scie. Tech.* 17, 777-785, ISSN: 0861-9786.
- MATLAB version 7.3 (R2006b). The MathWorks.
- Montgomery, D. O. (1997) *Design and Analysis of Experiments, 4th edn.* John Wiley and Sons, New York.
- Myers, R. H. & Montgomery, D. O. (1995) *Response Surface Methodology*, John Wiley and Sons Ed., ISBN: 0-471-41255-4 New York.
- Peñuelas, I., Rodríguez, C., Antuña, M., Betegón, C. & Lezcano, R. (2009). Caracterización mecánica de recubrimientos mediante ensayos miniatura de punzonamiento, *Actas del IX congreso iberoamericano de Ingeniería Mecánica*, sec 13, 25-31, ISBN: 978-84-692-8516-9.
- Rodríguez, C. et al (2009) Mechanical Properties Characterization of Heat-Affected Zone Using the Small Punch Test, *Welding journal*, 88, 9, 188-192, ISSN: 0043-2296.
- Seshadri, A. (2006). A fast elitist multiobjective genetic algorithm: NSGA-II. *MATLAB Central*.
- Stravroulakis, G. E., Bolzon, G. & Waszczyszyn, L. (2003). Inverse analysis. *Comprehensive Struct. Integrity.* 3, 1-34.
- Sun DZ, et al., (1992) Application of micro-mechanical models to the prediction of ductile fracture. *Fracture mechanics, 22nd symposium.* ASTM STP 1131, vol. II, 368-78.
- Tvergaard, V. (1981) Influence of voids on shear bands instabilities under plane strain conditions. *Int. J. Fract.* 17, 389-407, ISSN: 0376-9429.
- Tvergaard, V. (1982) On localization in ductile materials containing spherical voids. *Int. J. Fract.* 18, 157-169, ISSN: 0376-9429.
- Tvergaard, V. & Needleman, A. (1984). Analysis of cup-cone fracture in a round tensile bar. *Acta Metall.* 32, 57-169, ISSN: 0-56-7151.
- Tvergaard, V. (1990) Material failure by void growth to coalescence. *Adv. Appl. Mech.* 27, 83-151 ISBN: 0-12-002040.

IntechOpen



## **Numerical Simulations - Applications, Examples and Theory**

Edited by Prof. Lutz Angermann

ISBN 978-953-307-440-5

Hard cover, 520 pages

**Publisher** InTech

**Published online** 30, January, 2011

**Published in print edition** January, 2011

This book will interest researchers, scientists, engineers and graduate students in many disciplines, who make use of mathematical modeling and computer simulation. Although it represents only a small sample of the research activity on numerical simulations, the book will certainly serve as a valuable tool for researchers interested in getting involved in this multidisciplinary field. It will be useful to encourage further experimental and theoretical researches in the above mentioned areas of numerical simulation.

### **How to reference**

In order to correctly reference this scholarly work, feel free to copy and paste the following:

Ines Penuelas, Covadonga Betegon, Cristina Rodriguez and Javier Belzunce (2011). Inverse Methods on Small Punch Tests, Numerical Simulations - Applications, Examples and Theory, Prof. Lutz Angermann (Ed.), ISBN: 978-953-307-440-5, InTech, Available from: <http://www.intechopen.com/books/numerical-simulations-applications-examples-and-theory/inverse-methods-on-small-punch-tests>

**INTECH**  
open science | open minds

### **InTech Europe**

University Campus STeP Ri  
Slavka Krautzeka 83/A  
51000 Rijeka, Croatia  
Phone: +385 (51) 770 447  
Fax: +385 (51) 686 166  
[www.intechopen.com](http://www.intechopen.com)

### **InTech China**

Unit 405, Office Block, Hotel Equatorial Shanghai  
No.65, Yan An Road (West), Shanghai, 200040, China  
中国上海市延安西路65号上海国际贵都大饭店办公楼405单元  
Phone: +86-21-62489820  
Fax: +86-21-62489821

© 2011 The Author(s). Licensee IntechOpen. This chapter is distributed under the terms of the [Creative Commons Attribution-NonCommercial-ShareAlike-3.0 License](#), which permits use, distribution and reproduction for non-commercial purposes, provided the original is properly cited and derivative works building on this content are distributed under the same license.

IntechOpen

IntechOpen